This is a repository copy of *Effect of niobium supersaturation in austenite on the static recrystallization behavior of carbon structural steels*.

White Rose Research Online URL for this paper:
https://eprints.whiterose.ac.uk/188624/

Version: Published Version

Article:

Effect of Niobium Supersaturation in Austenite on the Static Recrystallization Behavior of Carbon Structural Steels

B. RAKSHE, J. PATEL, and E.J. PALMIERE

This work describes the effect of Nb supersaturation in austenite on the suppression of static recrystallization of austenite during an isothermal holding period following hot deformation. The investigation involved three carbon structural steels with varying Nb concentration at constant C (0.20 pct) and N (0.007 pct) levels. The isothermal double-hit deformation technique led to the determination of $T_{5\ \text{pct}}$ and $T_{95\ \text{pct}}$ (recrystallization-stop and full recrystallization temperatures, respectively) as a function of a true strain and interpass time. The results indicate that the $T_{5\ \text{pct}}$ increases with increasing Nb supersaturation in austenite at a rate of 40 °C per 0.006 pct Nb supersaturation for a true stain $\varepsilon = 0.40$. At each respective $T_{5\ \text{pct}}$, all tested steels exhibited an Nb supersaturation ratio ≥ 7.5 in austenite. A high, localized strain-induced precipitation of Nb(CN) was observed at the austenite subgrain boundaries in the unrecrystallized microstructure. This translated into higher values for local precipitate-pinning forces (F_{PIN}), which were significantly higher than that predicted from equilibrium thermodynamics. The critical F_{PIN} for retardation of static recrystallization was found to be 1.6 MPa at the respective $T_{5\ \text{pct}}$ for each steel. The present study has contributed to advancing our knowledge of the interplay between Nb solute supersaturation and volume fraction of Nb(CN) precipitation in particular for carbon structural steels. It has also highlighted an opportunity to apply niobium, even an ultra-low addition (*i.e.*, < 100 ppm) to commodity-grade structural steels to reduce overall alloying costs.

I. INTRODUCTION

THE principal role of niobium in the thermomechanical treatment of austenite is well established and industrially practiced for several decades towards the development of high strength steels, in particular the additions of small (micro) amounts of niobium to carbon-manganese steels. The main mechanisms at play being (i) precipitation of niobium carbonitride (Nb(CN)) particles in austenite during hot rolling, where the formation of fine precipitates significantly retards (delays) the recovery and recrystallization of austenite and subsequent grain growth prior to transformation, and (ii) precipitation of further finer Nb(CN) particles during austenite phase transformation and/or after that provide strengthening contribution from dispersion hardening.

The ability of niobium in retarding austenite recrystallization has been extensively researched and today is commonly accepted that this happens through the stages of (i) niobium atoms in solution, *i.e.*, a solute-drag effect, and (ii) strain-induced niobium carbonitride precipitates. The majority of investigations have shown that it is the latter mechanism that is by far dominant, with many suggesting that there is a critical precipitate supersaturation which is required for significant retardation to occur.[1–5] Others strongly advocate that it is a combination of the two mechanisms, especially as there has to be a point concentration of niobium atoms in the first instance to develop critical precipitate supersaturation,[5,6] while others have presented compelling cases for the solute-drag effect to have an equal level of importance.[7,8]

About half of the total steel produced worldwide goes into the building and infrastructure sector. As an example, 919 million tons of global crude steel was used in the construction sector for year 2019 accounting for 52 pct of overall world steel demand.[9] A significant portion of structural steels produced remain that of

B. RAKSHE is with JSW Steel Limited, Dolvi, Raigad 402107, India. J. PATEL is with International Metallurgy Ltd, Oxfordshire OX9 3DS, UK and also with CBMM Technology Suisse S.A., Geneva, 1207, Switzerland. E.J. PALMIERE is with the Department of Material Science and Engineering, The University of Sheffield, Sheffield S1 3JD, UK. Contact e-mail: e.j.palmiere@sheffield.ac.uk

conventional plain C-Mn variety with relatively low yield strengths ranging from 235 to 355 MPa even with advances in the steel-processing technologies. Today, the construction industry is facing significant challenges in developing sustainable structures using a cost-effective method especially within the built environment. Consequently, the structural engineering community is now increasingly using advanced high strength steel (HSS) grades for building lighter and stronger fabrications as well as composite structures to overcome these challenges. It is well known that HSS has a higher load-bearing capacity due to its higher yield strength compared to equivalent mild-steel grades, which reduces the weight of the structure, and total cost saving in a range of 10 to 30 pct is possible through weight reduction and associated benefits.[10,11]

Structural steels typically have a carbon content between 0.15 and 0.20 wt. Pct C which limits the solubility of Nb in austenite at hot deformation temperatures. Therefore, higher soaking temperatures are often required to fully utilize Nb precipitation potential in controlled rolling of austenite for typical structural steels. However, many commodities-grade structural long product steel producers use lower soaking temperature ($T_S \leq 1150$ °C) and hot charging of billets to save in energy costs. In effect, the amount of Nb available in austenite solution and its precipitation contribution can be restricted by lower reheating practices and finish-rolling temperatures near and above 950 °C. Therefore, the use of conventional Nb-microalloying technology has been somewhat limited with mainstream commodity structural steels and only when higher yield strengths, ≥ 350 MPa, or heavy sections or plates are required. Evidence suggests that lower Nb additions (100 to 150 ppm) can have a beneficial effect on the mechanical properties of structural steel long products.[12–14] Small Nb additions suppress static recrystallization under certain rolling conditions for some steel products.[15,16] However, many of these investigations lacked detailed analysis and mechanism as to the role of Nb at these lower additions in such low-strength commodity structural steel grades, where Nb is not traditionally applied.

The purpose of this paper is to contribute to the understanding of low (*i.e.,* 100 to 200 ppm Nb) and what is termed ultra-low (*i.e.,* ≤100 ppm) additions of niobium on pinning forces (F_{PIN}) developed by strain-induced precipitation towards the retardation of austenite recrystallization in typical carbon structural steels. The main goal was to measure and understand the differences in F_{PIN} resulting from a volume fraction of Nb(CN) localized around austenite subgrain boundaries. The measured pinning force was subsequently related to the results of the fractional softening studies and solute supersaturation of Nb in the austenite at a given deformation temperature.

Table I. Chemical Composition of the Experimental Heats in Wt Pct

Element	C	Mn	Si	P	S	Nb	N
B0/Base	0.20	1.03	0.20	0.018	0.008	0.0000	0.0058
B1	0.20	1.03	0.19	0.018	0.008	0.0066	0.0056
B2	0.20	1.01	0.19	0.015	0.007	0.0121	0.0074
B3	0.20	1.01	0.19	0.015	0.007	0.0214	0.0070

II. EXPERIMENTAL PROCEDURE

A. *Material Processing*

A series of carbon structural steels were designed to have a different precipitation supersaturation by varying the Nb concentration (50 to 200 ppm) for a constant level of a carbon composition (0.20 pct C). Table I gives the chemical composition of these experimental heats. All the steels were vacuum induction melted and ingot cast (30 kg each) in the former Swinden Technology Centre of Tata Steel. The as-cast ingots were subsequently rolled to refine the as-cast microstructure and to produce material of suitable gage for subsequent machining of plane strain compression (PSC) test specimens. The ingots were homogenized at 1300 °C and hot rolled down to plates of 25 mm (T) $\times$ 105 mm (W) $\times$ 1500 mm (L) size in multiple passes.

It is essential to dissolve the Nb(CN) precipitates back into solid solution and restore a fully equiaxed microstructure prior to hot deformation studies. Hence, the as-rolled plates were homogenized at 1250 °C for 1 hour in a box furnace filled with N_2 atmosphere. The reheating temperature of 1250 °C was predetermined from published solubility equation of Irvine *et al.*[17] for complete dissolution of Nb in austenite solution. Immediately following a soak time, specimens were quenched in a tank filled with ice water so that the composition of austenite at 1250 °C could be retained. After cooling down to room temperature, the PSC specimens of rectangular geometry having a dimension of 10 mm $\times$ 30 mm $\times$ 60 mm were machined from homogenized plates.

B. *Static Softening Studies*

The isothermal hot deformation studies were conducted under a constant true strain rate condition using a purpose-built thermomechanical compression (TMC) machine at The University of Sheffield, UK. Figure 1 illustrates the temperature–time experiment schedule designed to measure the overall softening of austenite under a prescribed delay time (t_D) of 5 and 20 seconds. Each specimen was coated with a boron nitride (BN) to minimize adverse friction effects and sticking during the hot deformation studies.

The PSC specimen was again reheated to 1250 °C within an inductive heating system of TMC machine and held for 2 minutes to allow for equilibrium within the specimen. Following the hold time, the reheated specimen was forced air-cooled at a rate of 20 °C/s to one of the five deformation temperatures (1050 °C, 1000 °C, 950 °C, 900 °C, and 850 °C) and immediately transferred to test furnace for hot deformation. The hot deformation was immediately undertaken in a double pass of the equal magnitude of a true strain from $\varepsilon_1 = \varepsilon_2 = 0.40$ with a hold time of 5 and 20 seconds in between two passes. The deformed specimen was instantly water quenched to room temperature (quench time 1 to 1.5 seconds) after the second deformation pass (ε_2). A constant strain rate of 15 s^{-1} was applied during the deformation passes. An uninterrupted deformation was also carried out for total strain $\varepsilon = \varepsilon_1 + \varepsilon_2 = 0.80$ without any intermediate holding time at selected temperature for each steel.

C. Recrystallization and Grain Size Measurements

The hot deformation under PSC condition is assumed homogeneous across the specimen thickness in theory; however, inhomogeneities exist in the strain, strain rate, and temperature distribution. Mirza et al.[18] studied the effect of frictional conditions and initial specimen geometry on strain distribution in a PSC testing. The central deformation regions represent applied plastic strain; hence, microstructure characterization was focused only on the central area of 0.5 to 1.0 mm^2 along the rolling-normal direction (RD-ND). The strain inhomogeneities in industrial rolling conditions are far higher than those observed under PSC deformation on the TMC.

The metallographic preparation was carried out using a standard grinding and polishing technique on double-hit specimens. The prior-austenite grain boundaries (PAGB) were revealed using a solution of saturated picric acid at 85 to 90 °C.[19,20] The mean prior-austenite grain size and aspect ratio were measured using an optical microscope. The linear intercept grain sizes $\overline{L}_1$ and $\overline{L}_3$ were measured from the counts in RD and ND directions, respectively, after the second hit deformation cycle. The means PAGS $(\overline{L}_1 * \overline{L}_3)^{0.5}$ and aspect ratio $(\overline{L}_1/\overline{L}_3)$ were calculated assuming an axial symmetry of the grains from the above measurements.[21]

D. Nb(CN) Precipitate Measurements

For Nb(CN) precipitate observations, PSC specimens were deformed to initial true strain, $\varepsilon_1 = 0.40$ in a single-hit cycle, isothermally held for 20 seconds, followed by immediate water quenching. Quantitative electron microscopy was performed to determine size and volume fraction of Nb(CN) precipitates. Carbon extraction replica and thin foils samples were prepared with standard five-stage process and subsequently analyzed in FEI Tecnai 20 and JEOL 2010 analytical electron microscopes. Energy dispersive X-ray (EDX) analysis and electron energy loss spectroscopy (EELS) were performed on Nb(CN) precipitates to determine their chemical composition at a spot along a line or in a particular area.

The mean diameter of the precipitate and its confidence limits were determined directly from precipitate size measurements over multiple locations in the carbon extraction replica using the ImageJ software. An average of 100 particles were measured to determine the precipitate size distribution in the planar section. The number of precipitates per unit area (N_s) and per unit volume (N_V) were calculated using Woodhead analysis method.[21] The volume fraction of Nb(CN) precipitates (f_v) was then calculated according to the method of
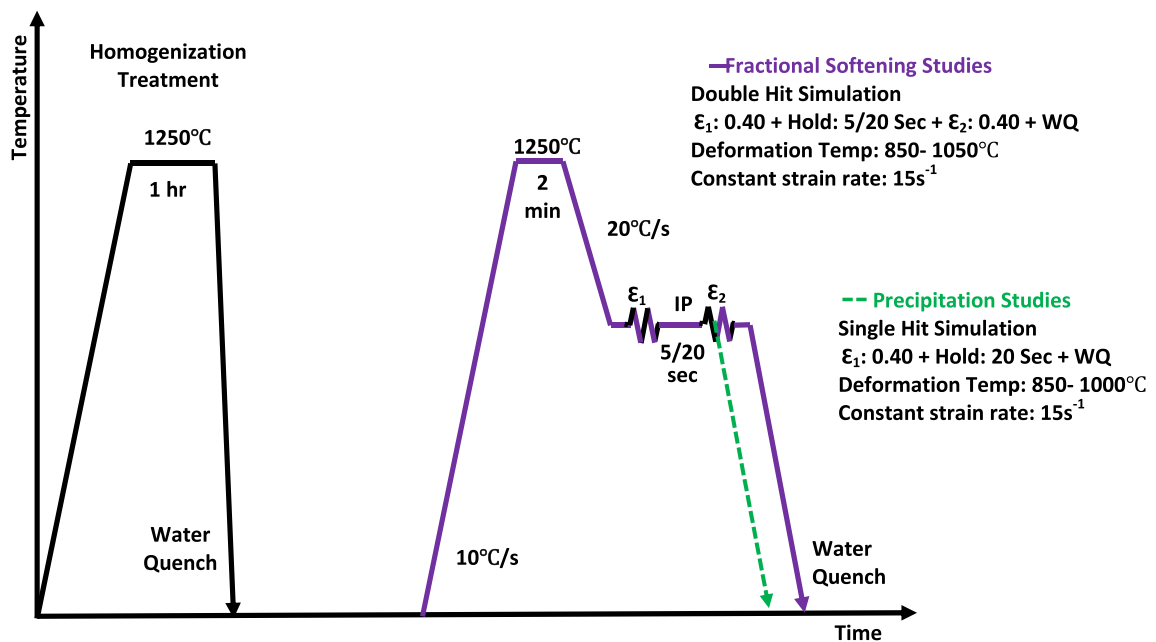

Fig. 1—Time–temperature schedule designed to measure static softening of austenite of steel B0–B3.

Ashby and Ebling[22] assuming extraction of spherical particles from replica:

$$f_v = \tfrac{\pi}{6} N_s \left(\bar{x}^2 + \sigma^2 \right) \qquad [1]$$

where N_s is the number of particles per unit area and $\bar{x}$ is the planar arithmetic mean and σ is the standard deviation.

III. RESULTS

A. Fractional Softening Studies

The raw load–displacement data were converted into equivalent stress–strain flow curves using a guide for the best practice developed at The University of Sheffield in collaboration with the National Physical Laboratory in the UK.[23] The instantaneous temperature of specimen rises by 20 to 30 °C for the strain rate of $15s^{-1}$ during the hot deformation. The temperature rise during the deformation is not adiabatic, and the flow stress has to be corrected to represent true isothermal test condition.[23] The corrected isothermal stress (σ_{iso}) is used for estimation of fractional softening of austenite.

Figure 2 shows the high-temperature flow curves from the uninterrupted compression tests at different deformation temperatures for a true strain, $\varepsilon = 0.80$. The amount of stress increases with decreasing deformation temperature for a given strain level and at a constant strain rate, consistent with the Zener–Hollomon relationship.[24] Another notable feature is that there was no evidence of dynamic recrystallization resulting from the deformation conditions used in this research. This observation is important in that the fractional softening measured from the double-hit test will be exclusive of the static restoration events (*i.e.,* recovery and recrystallization) during the hold time.

The percent fractional softening of austenite is measured from area under flow stress curves as a function of an isothermal temperature and hold time. The fractional softening parameter, X_A, first used by Kwon et al.,[25] has been adopted in this present study. The details of this technique and the method of calculation are described elsewhere.[3,4,19,25] The expression of X_A is given as follows:

$$X_A = \frac{A_3 - A_2}{A_3 - A_1} \qquad [2]$$

where A_1 is the common area under the flow stress between the first deformation in an interrupted test and the part in the monotonic test to the same prestrain level. A_2 is the area under the flow curve of the second deformation in the interrupted compression test, while A_3 is the area under the flow curve in the monotonic test over the strained region equivalent to the second deformation in the interrupted tests.

Figure 3 graphically depicts the percent fractional softening behavior during the 5 and 20 seconds hold times for all steel as a function of deformation temperature. As expected, the amount of fractional softening observed for each steel increased with increasing deformation temperature. For steels, B0-B3 softening curves

exhibited a typical sigmoidal shape with three distinct stages. The rate of fractional softening was initially slow (Stage I: static recovery), rising at an intermediate stage (Stage II: partial static recrystallization), and decreased as the static recrystallization proceeded to completion (Stage III: full recrystallization) for each steel.

The amount of fractional softening measured during PSC tests corresponds to the total net softening of austenite during the hold times of 5 and 20 seconds, respectively. Hence, the total net softening is considered to compose of all static restoration and/or strengthening events: softening due to recovery and recrystallization, as well as hardening due to precipitation. The fraction softening due to static recovery would be small in these steels because the stacking fault energy of austenite is relatively low (75 mJ/m^2) and would, therefore, have more difficulty of dislocation cross-slip.[3,4,19] Therefore, the overall softening behavior presented in Figure 3 largely represents the softening due to static recrystallization of austenite.

The observed plateau of initial softening in stage I (up to 20 pct total fractional softening) is attributed to recovery process alone. This result is in agreement with findings from previous investigators[3,4,26,27] who had also observed 20 pct of softening due to recovery. Beyond this regime, further softening is attributed to static recrystallization of austenite for a set hold time of 5 and 20 seconds. The $T_{5\ pct}$ (recrystallization-stop temperature) for each steel composition was determined from Figure 3 by employing criteria that 20 pct of total softening is due to recovery of austenite.

The $T_{5\ pct}$ results are shown in Figure 4 for steel B0-B3. The $T_{5\ pct}$ increases with increase in amount of Nb added to base steel in the following order: 820 °C (0Nb), 855 °C (0.007 pct Nb), 894 °C (0.012 pct Nb), and 943 °C (0.021 pct Nb) for a hold time of 20 seconds,. For steel B3, measured $T_{5\ pct}$ is 120 °C higher than B0 (base grade) which is significant considering that it has only 200 ppm level of Nb addition. As
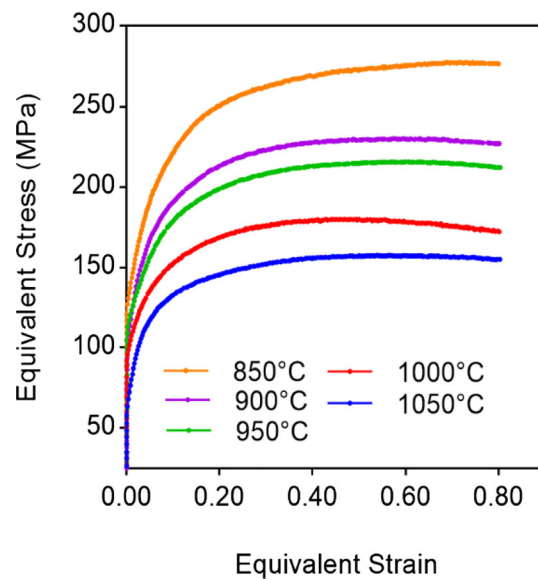

Fig. 2—Flow stress for steel B1 at different deformation temperatures during uninterrupted deformation ($\varepsilon = 0.80$). A constant true strain rate of 15 s^{-1} was applied.
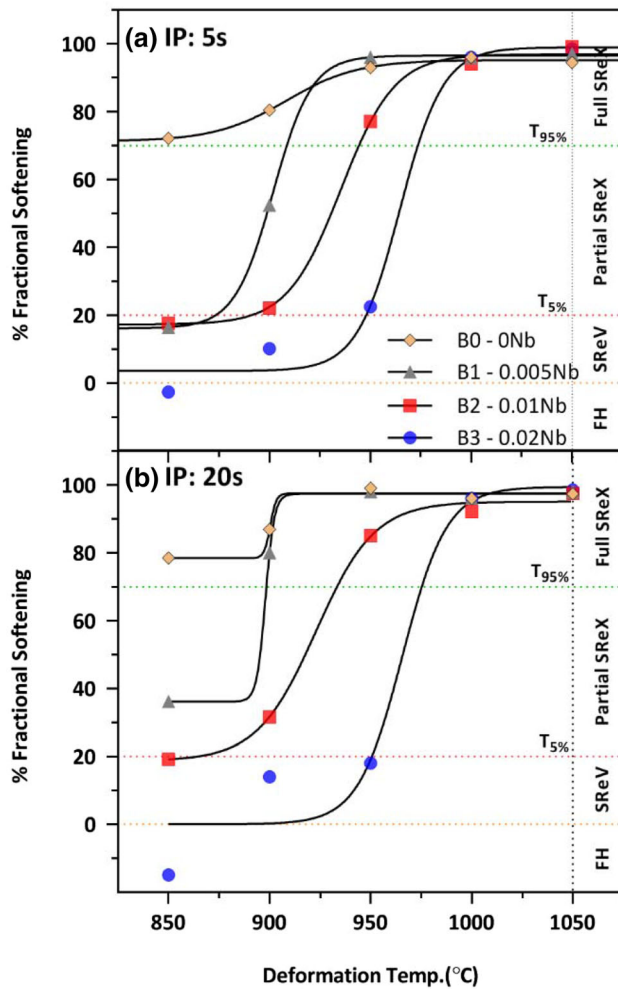
Fig. 3—Percent fractional softening of austenite versus deformation temperature for steel B0–B3 as determined from interrupted compression testing (FH: Fractional Hardening, SReV: Static Recovery, Partial SReX: Partial Static Recrystallization and Full SReX: Full Static Recrystallization).

austenite restoration is thermally activated process, measured $T_{5\ pct}$ for a hold time of 5 seconds was marginally higher (5 to 10 °C) than 20 second hold time.

As the deformation temperature increased, accelerated recrystallization kinetics were observed which might be due to reduced Nb(CN) precipitation potential at the higher temperature. Therefore, the convergence of softening curves above 70 pct fractional softening value is indicative of complete static recrystallization. The $T_{95\ pct}$ (recrystallization-limit temperature) for each steel was then determined corresponding to 70 pct of overall softening of austenite. The $T_{95\ pct}$ temperature also increases as Nb increases for steel B0–B3: 881 °C (0Nb), 908 °C (0.007 pct Nb), 944 °C (0.012 pct Nb), and 980 °C (0.021 pct Nb). The fraction-softening results show that the window of partial recrystallization is highest for steel B0 (70 °C) while lowest for steel B3 (30 °C) for both hold times.

The results shown in Figures 3 and 4 are unique in that the fractional softening of austenite is measured as a function of deformation temperature at a constant

delay time. The five deformation temperatures (850 °C to 1050 °C) selected in this study represent the typical finish-rolling processing window for the long products. Similarly, the holding time of 5 and 20 seconds was chosen to represent an industrial rolling practice for light to heavy sections as well as plate mills.

B. Microstructure Studies: PAGS

Figure 5 shows the microstructure of steel B0–B3 after reheating to the temperature of 1250 °C for 1 hour and followed by immediate water quenching. All microstructure appears to be fully martensite, mostly a lath structure. There was no indication of pro-eutectoid ferrite formation along the PAGB. The mean prior-austenite grain sizes (PAGS) of steel B0–B3 were in the range of 140 to 165 μm.

The fractional softening data in Figure 3 were further complemented using quantitative metallography. This was necessary to verify the correspondence between 20 pct fractional softening and $T_{5\ pct}$ criteria. Excellent agreement is obtained between microstructure and fraction-softening data from the compression tests. At temperatures below $T_{5\ pct}$ for each steel, the prior-austenite grains were completely unrecrystallized. These deformed grains were elongated in a direction, which was perpendicular to the axis of compression. At temperatures above the respective $T_{95\ pct}$ for each steel, the prior-austenite grains were completely recrystallized, i.e., consisting of small equiaxed grains.

Figure 6 shows the series of microstructures of steels B1 [Figures 6(a) through (d)], B2 [Figures 6(e) through (h)], and B3 [Figures 6(i) through (l)] exhibiting this behavior for different deformation temperatures, respectively. These samples were subjected to a single-hit cycle of strain, $\varepsilon = 0.40$, isothermal hold time of 20 seconds
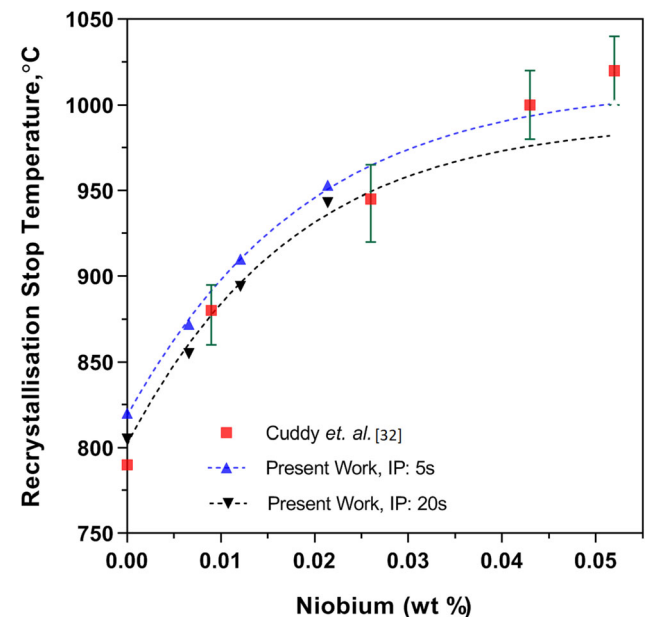

Fig. 4—Effect of initial Nb content on recrystallization-stop temperature ($T_{5\ pct}$) of steel B0–B3 (reproduced from Ref. 32).

followed by immediate water quenching. As an example, the microstructure corresponding to a deformation temperature of 950 °C reveals a completely unrecrystallized prior-austenite grain structure [Figure 6(k)] in steel B3. The microstructure corresponding to a deformation temperature of 1000 °C indicates a completely recrystallized austenite microstructure [Figure 6(l)]. The $T_{5 \text{ pct}}$ and $T_{95 \text{ pct}}$ for steel B3 were measured as 953 °C and 980 °C, respectively, from interrupted compression testing. The sequence of microstructures validates the finding from the softening studies that temperature range ($T_{5 \text{ pct}} < T_{\text{def}} < T_{95 \text{ pct}}$) where partial recrystallization can occur is very narrow for steel B3, no greater than 30 °C.

The recrystallization-driving forces and precipitate-pinning forces are of comparable magnitude in steel B3 due to higher Nb supersaturation in austenite which has led to very narrow recrystallization region in steel B3 in comparison to steel B1 and B2. The experimental evidence for this observation will be discussed in the following sections based upon actual measurements of F_{RXN} and F_{PIN} at different deformation temperatures and the subsequent interaction between them.

Figure 7 shows the mean prior-austenite grain size (PAGS) and aspect ratio for steels B0 to B3 as a function of deformation temperature after double-hit compression tests. These parameters were taken as indicators of the degree of recrystallization or work hardening of the austenite grains. For example, the mean PAGS of unrecrystallized austenite was in the range of 130–150 μm while recrystallized austenite exhibited the mean PAGS of 25 to 35 μm. At temperatures below $T_{5 \text{ pct}}$, steel B0–B3 exhibit an aspect ratio in the range of 10 to 20, signifying an elongated or unrecrystallized austenite microstructure. At temperatures above the $T_{95 \text{ pct}}$, all steel has aspect ratio of approximately 1.1 to 1.2, signifying a fully recrystallized austenite microstructure. At intermediate deformation temperature, the variation in aspect ratio was observed.

C. Electron Microscopy: Nb(CN) SIP

Figure 8 shows the TEM micrograph depicting Nb(CN) precipitates in steel B3 which was deformed in single hit at 950 °C, $\varepsilon = 0.40$ and isothermally hold for 20 sec followed by immediate water quenching. The microstructure is characteristic of low-carbon martensite ($\acute{\alpha}$) and often referred to as lath martensite due to lath or plate-like morphology [Figure 8(a)]. The lath thickness of the microstructure was found to be 0.20 to 0.50 μm. The dark-field TEM micrograph of same area revealed localized non-random Nb(CN) precipitation in linear arrays manner at the austenite grain boundaries [Figure 8(b)]. The selected area diffraction pattern (SADP) analysis revealed the orientation relationship between the Nb(CN) precipitates and quenched martensite matrix [Figure 8(c)]. The close-packed directions from both the precipitate and matrix were found to be parallel, $[110]_{\text{NbC}} // [111]_{\acute{\alpha}}$. The observed precipitate exhibits a Kurdjumov–Sachs (KS) orientation relationship with the matrix which signifies that precipitates were formed in hot-deformed austenite as a function of applied strain. The precipitates were identified by EDX at multiple locations [Figure 8(d)]. The observed Nb L_{α} peaks confirm that precipitate is Nb rich and can be considered as Nb(CN).

Figure 9 shows the bright-field TEM micrographs depicting morphology of strain-induced Nb(CN)
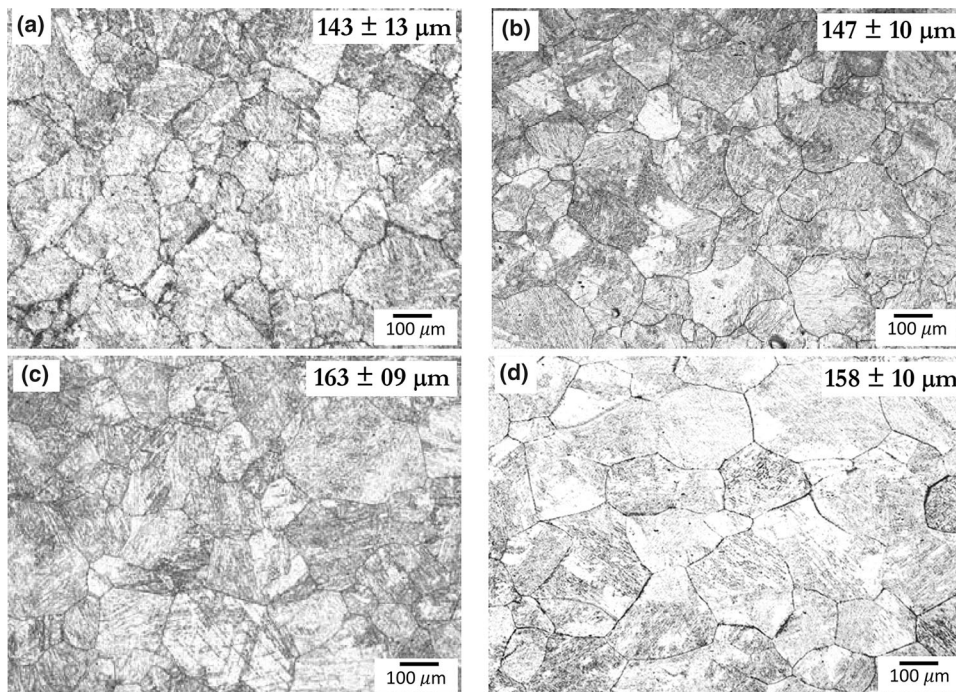
Fig. 5—Microstructure of steel (a) B0, (b) B1, (c) B2 and (d) B3, respectively, which were reheated to 1250 °C, isothermally hold for 1 h and WQ. The prior-austenite grain sizes were revealed by etching with saturated picric acid solution.
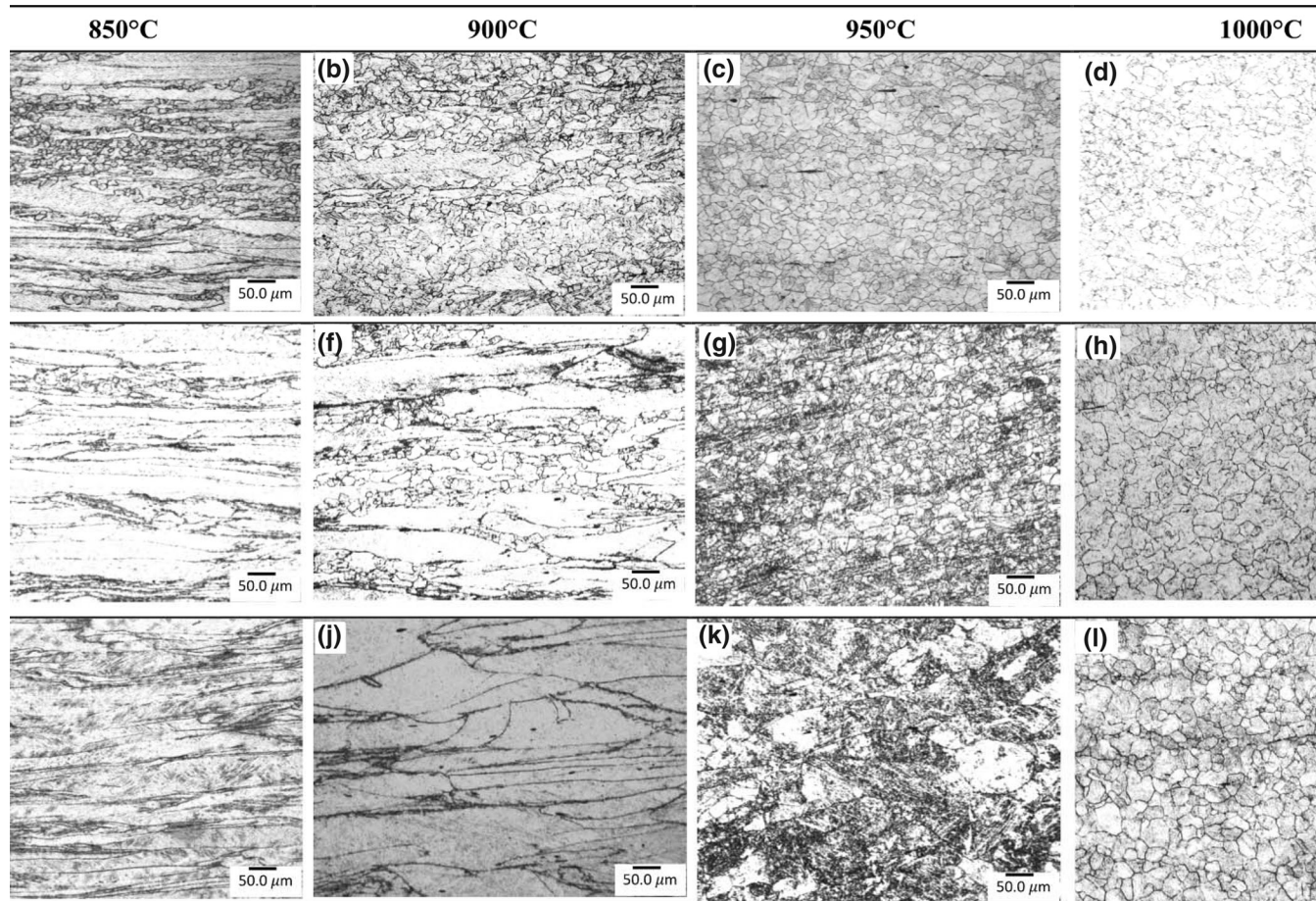
| 850°C | 900°C | 950°C | 1000°C |

Fig. 6—Microstructure evaluation in steel B1–B3 at the respective deformation temperature: (*a*) through (*d*) Steel B1, (*e*) through (*h*) Steel B2, and (*i*) through (*l*) Steel B3. The microstructure was obtained after a single-hit deformation at strain $\varepsilon = 0.40$, an isothermal hold of 20 s, and WQ. The constant strain rate of $15s^{-1}$ was applied. Based on fractional softening studies, steel B1–B3 had a $T_{5\ pct}$ of 855 °C (0.007 pct Nb), 900 °C (0.012 pct Nb), and 943 °C (0.021 pct Nb), respectively.

precipitation in steel B1 [Figures 9(a) through (d)], B2 [Figures 9(e) through (h)], and B3 [Figures 9(i) through (l)], respectively. The samples were deformed at 850–1000 °C, $\varepsilon = 0.40$, and isothermally hold for 20 seconds followed by immediate water quenching. The micrographs show evidence of precipitates in a close proximity to remnant of austenite subgrain boundaries. The lognormal particle size distribution was observed for all deformation test conditions with a mean particle sizes range from 15 to 30 nm. The measured particle size and distribution were typical of Nb(CN) strain-induced precipitation in low-carbon-microalloyed steels. The EDX spectrum demonstrated that these particles contain predominately Nb, C, and N elements.

The precipitate location is essential, as they provide much more grain boundary pinning potential if they are located on austenite subgrain boundaries rather than located randomly throughout the matrix. An example of this localized precipitation is shown in Figures 8 and 9 which seems to be typical nature of strain-induced Nb(CN) precipitation in deformed austenite. This behavior has been reported in numerous investigations on a low-carbon Nb-microalloyed steels over the last five decades.[1–4,28,29]

Table II summarizes the quantitative measurement of precipitate size, volume fraction, and corresponding F_{PIN} from multiple TEM images shown in Figure 9. The result shows that the precipitate formed at lower deformation temperature (high Z condition) is finer compared to one formed at higher temperature (low Z condition) in steel B1–B3. The precipitation kinetics behavior of Nb(CN) in steel B1–B3 is similar; however, the observed volume fraction in steel B3 is significantly higher than steel B1 and B2.

Quantitative measurement further indicates that the volume fraction of strain-induced Nb(CN) precipitates increases with decreasing deformation temperature, irrespective of whether precipitation had occurred locally on the grain boundary or in the matrix. This behavior is illustrated for steels B1–B3 in Figure 10. The experimentally measured volume fraction, $f_{v\ (EXP)}$, can be further compared to what would have been predicted from thermodynamic calculation. The equilibrium volume fraction, $f_{v\ (EQM)}$, was calculated using a mass balance approach with assuming a fixed stoichiometry in Nb(CN) precipitation.[30,31] A comparison between $f_{v\ (EXP)}$ and $f_{v\ (EQM)}$ values for steels B1 to B3 is shown in Figure 10. It is clear from Figure 10 that the $f_{v\ (EXP)}$ is
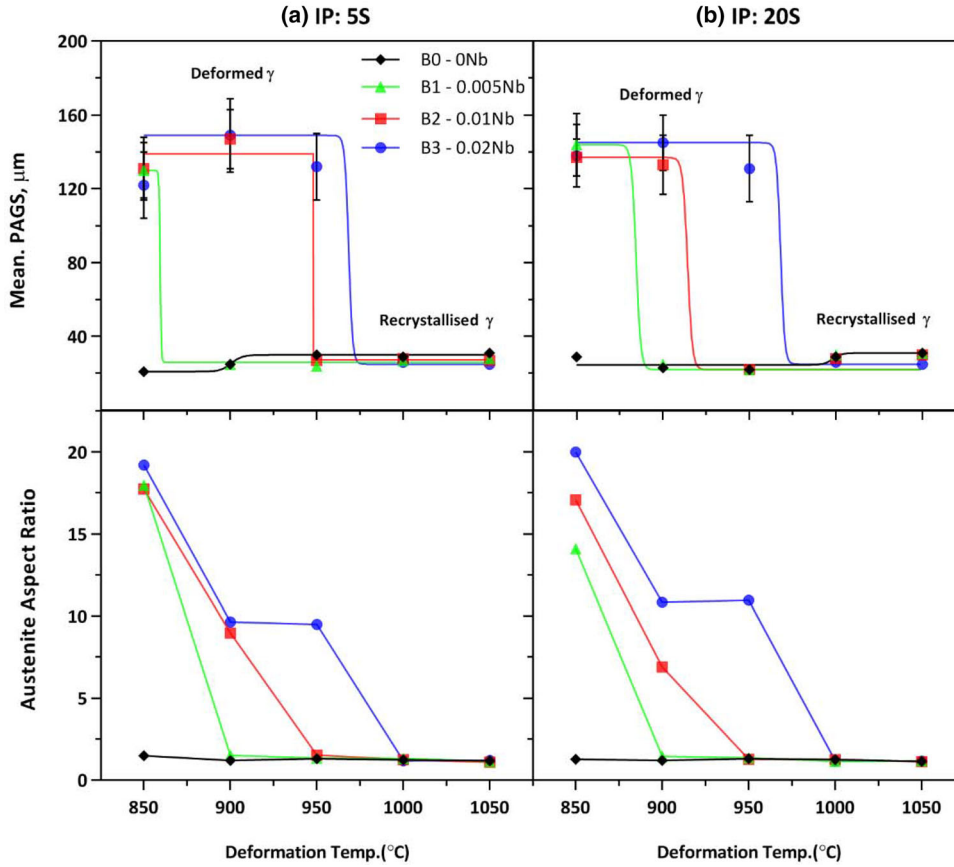
Fig. 7—Mean PAGS and aspect ratio of steel B0–B3 (*a*) IP: 5 s and (*b*) IP: 20 s as a function of deformation temperature after double-hit compression testing at strain: $\varepsilon_1 = \varepsilon_2 = 0.40$. All tests were carried out at a constant strain rate of 15 s^{-1}.

around 4 to 10 times higher than $f_{v\ (EQM)}$ at any given deformation temperature for all steel.

IV. DISCUSSION

A. *Influence of Nb(CN) Supersaturation Ratio on $T_{5\ pct}$*

A very agreeable result is obtained between the $T_{5\ pct}$ obtained from the present investigation vs Cuddy's original results as shown in Figure 4. Cuddy's[32] experiments involved multi-pass rolling on low-carbon steels with total strain, $\varepsilon = 1.0$ (5 × 0.20) at different temperature while the present study had two deformation passes with total strain $\varepsilon = 0.80$ (2 × 0.40). However, the strain rates, interpass time, and method of deformation were similar, which is one of the main reasons for the favorable agreement. The results also show that the window of partial recrystallization is highest for steel B0 (70 °C) while lowest for steel B3 (30 °C) for both hold times.

The base composition (0.20C-1.0Mn-0.20Si) in these steels was chosen to represent typical levels in structural steel grades for beams sections and rebar applications. Steel B1–B3 displayed three different forms of Nb in the austenite solid solution at any given temperature if similar reheating and deformation conditions are applied. Accordingly, Nb(CN) precipitation behavior

in hot-deformed austenite should be different within steel B1–B3 due to systematic variation of Nb supersaturation in austenite, [Nb]$_{SS}$ at respective deformation temperature.[1–5]

[Nb]$_{SS}$ is given by solubility product, $k_s = $ [Nb][C] where [Nb] and [C] are the concentration of Nb and C dissolved in the austenite.[3,4] Nb supersaturation ratio in austenite, [Nb]$_{SSR}$, is defined as being the ratio of the solubility product of Nb(CN) in austenite at reheating temperature to the solubility product of austenite at the deformation temperature. Irvine *et al.*[17] solubility equation allows the calculation of [Nb]$_{SS}$ and [Nb]$_{SSR}$ using the following relation:

$$[Nb]_{SS} = [Nb]_{\gamma} - [Nb]_{\varepsilon} \qquad [3]$$

$$[Nb]_{SSR} = [Nb]_{\gamma} / [Nb]_{\varepsilon} \qquad [4]$$

where the term [Nb]$_{\gamma}$ and [Nb]$_{\varepsilon}$ represent the amount of Nb in solution at the respective reheating and deformation temperatures. Table III shows the estimated values [Nb]$_{SS}$ and [Nb]$_{SSR}$ at the respective deformation temperature for each steel composition.

Some interesting behaviors can be noted after combining the fractional softening data presented in Figure 3 with Table III. The suppression of austenite recrystallization is not associated with a unique [Nb]$_{SS}$
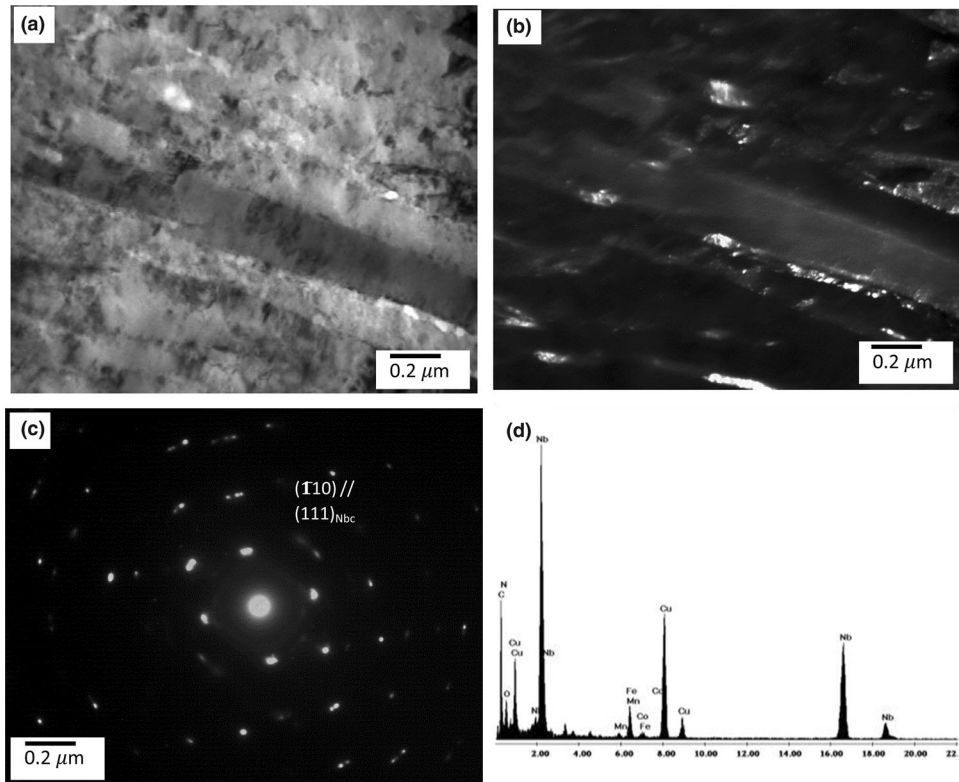
Fig. 8—TEM micrographs for steel B3 (0.021 pct Nb) which was deformed at 950 °C, strain ε = 0.40, isothermally hold for 20 secs followed by immediate water quenching: (*a*) bright-field TEM micrograph of Nb(CN) precipitates, (*b*) dark-field TEM micrograph of (a) depicting Nb(CN) precipitation along austenite subgrain boundaries, and (*c*) selected area diffraction pattern of precipitate and (*d*) corresponding EDS spectrum.

and varies for each steel at the respective $T_{5\ pct}$ as shown in Figure 11. However, an interesting trend can be observed that increasing $T_{5\ pct}$ is associated with increasing $[Nb]_{ss}$ in the austenite. An earlier investigation[1,2] had suggested that a critical degree of $[Nb]_{ss}$ must be exceeded for profuse the strain-induced Nb(CN) precipitation which then retards austenite recrystallization at $T_{5\ pct}$ temperature. Palmiere *et al.*[4] found that a $[Nb]_{ss}$ was not constant at respective $T_{5\ pct}$ and was dependent on the initial steel composition. He observed that a $[Nb]_{ss}$ ranged from 0.019 to 0.045 wt pct at respective $T_{5\ pct}$ for a series of low-carbon Nb-microalloyed steels. The present result is in favorable agreement with both the above findings with the view that retardation of recrystallization is not associated with unique a $[Nb]_{ss}$.

In previous investigation, it was suggested that the suppression of static recrystallization was associated with a similar $[Nb]_{SSR}$ in austenite.[1] Accordingly, the two steel compositions exhibited an $[Nb]_{SSR}$ of 7.5 and 5.0 when reheated at 1250 °C, deformed at 950 °C in a single pass of strain, $\varepsilon = 0.70$. Hence, Hansen *et al.* proposed a critical $[Nb]_{SSR}$ limit in between these values to retard static recrystallization through strain-induced precipitation.[1] In the present investigation, the static recrystallization was retarded for steels B1 to B3; whenever, the $[Nb]_{SSR} \geq 7.5$ for any given deformation temperature showing a favorable agreement with work of Hansen *et al.*[1] Figure 12 highlights the relationship between $[Nb]_{SSR,}$ and percent fractional softening for

steel B1 to B3 at respective deformation temperature. Steel B3 exhibited a $[Nb]_{SSR}$ of 7.8 at its respective $T_{5\ pct}$ (*i.e.*, 953 °C). It was obvious that a $[Nb]_{SSR}$ of 5.1 in steel B2 at 950 °C was not sufficient to retard complete recrystallization resulting in partial recrystallization.

Cuddy *et al.*[33] calculated the $[Nb]_{SSR}$ ratio at the respective $T_{5\ pct}$ for several steels which were simulated in multi-pass deformation on a laboratory rolling mill. These steels were soaked at several temperatures (950 to 1200 °C) to obtain range of initial solute Nb levels and $[Nb]_{SS}$. The observed $[Nb]_{SSR}$ at respective $T_{5\ pct}$ was not constant and ranged in value between 5 and 40. He reported the uncertainty in his results because soluble Nb was calculated from published solubility product of Nordberg *et al.*[34] However, he calculated $[Nb]_{SSR}$ as a ratio of solubility product (k_s) at reheating and deformation temperatures which could have given overestimated values of $[Nb]_{SSR}$. The recalculation of $[Nb]_{SSR}$ based on Irvine *et al.*[17] solubility product gives values in range of 3.10–6.20 at respective $T_{5\ pct}$. The modified results of Cuddy *et al.*[33] investigation compare favorably with the results of the present study.

During high-temperature deformation, recrystallization and precipitation are competing processes and the rate of each process depends upon which is occurring preferentially. Precipitation is the one which is significantly influenced by available $[Nb]_{ss}$ prior to deformation at any given deformation temperature. As highlighted earlier, static recrystallization suppression is not associated with unique $[Nb]_{ss}$; however, a constant

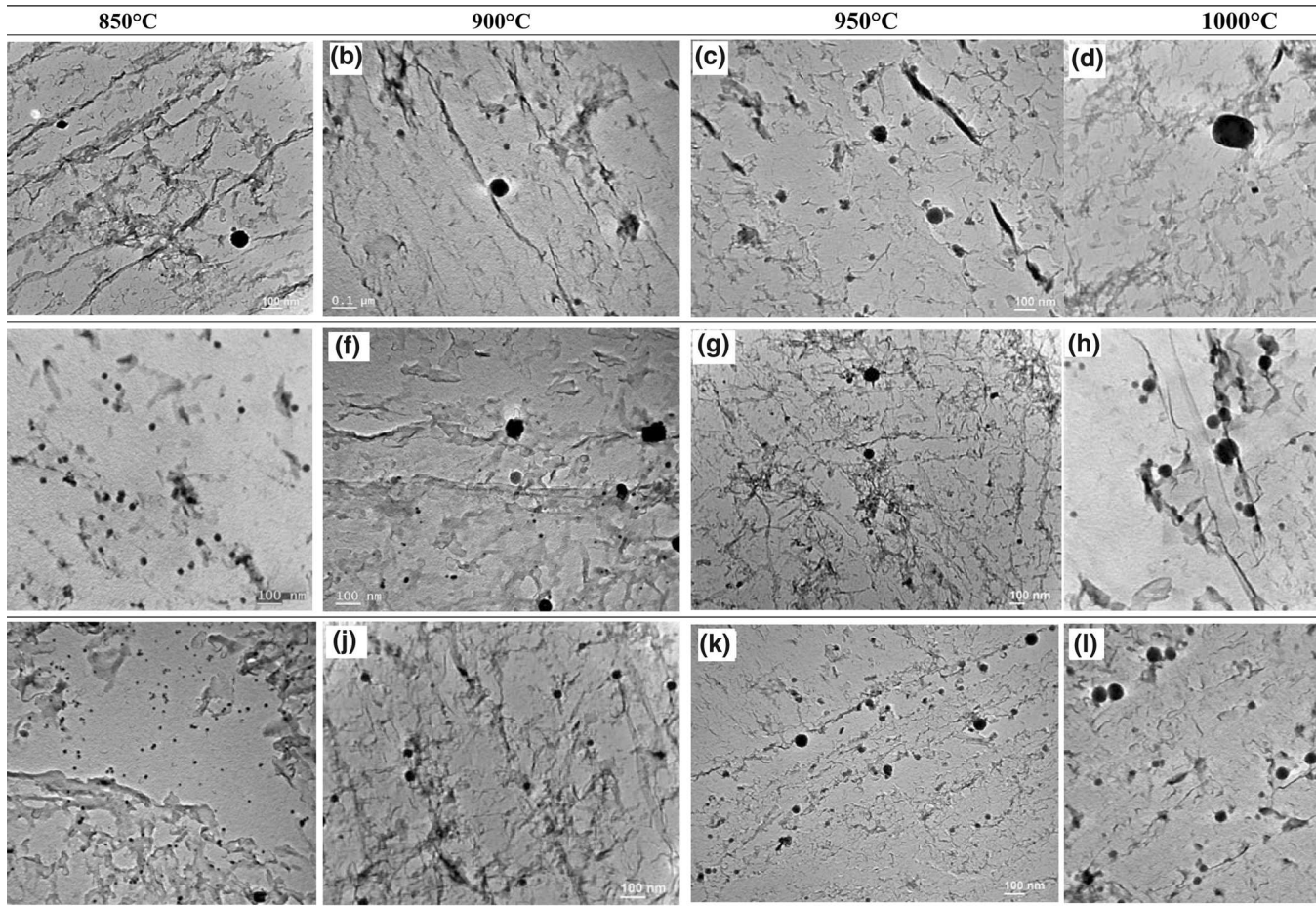| 850°C	900°C	950°C	1000°C

Fig. 9—TEM micrographs depicting Nb(CN) precipitation along austenite subgrain boundaries in steel B1–B3 at various deformation temperatures: (a) to (d) Steel B1, (e) to (h) Steel B2, and (i) to (l) Steel B3. All the samples were deformed in a single hit for a true strain, ε = 0.40, isothermally held for 20 s, and immediately water quenched.

[Nb]$_{SSR}$ was observed at each respective $T_{5\ pct}$ in the present study. It is expected that there will be sufficient volume fraction of Nb(CN) precipitates at the critical [Nb]$_{SSR}$, leading to the necessary pinning force to inhibit the recrystallization kinetics. The experimental evidences backing these observations are discussed in following sections.

B. Interaction Between F_{RXN} and F_{PIN}

In the present study, the use of a well-controlled TMC machine and PSC test enabled the more accurate determination of the increase in flow stress ($\Delta\sigma$) and corresponding change in the dislocation density (Δp). The F_{RXN} was calculated according to strain-induced boundary grain motion (SIBM) model which is a widely accepted recrystallization nucleation mechanism.[4,6,35] This model was originally put forth by Beck and Sperry[36,37] and was subsequently advanced through work of Bailey and Hirsch.[38] The shear modulus of austenite and the average burger vector were, respectively, assumed to be 4×10^4 MPa[1] and 2.5×10^{-10} m.[39] Figure 13 shows the variation of both precipitate-pinning force (F_{PIN}) and driving force for recrystallization, (F_{RXN}) with deformation temperature.

The curve for F_{RXN} in Figure 13 showed strong dependence on deformation temperature as the recrystallization is a thermally activated process. The $\Delta\rho$ is directly influenced by the deformation temperature; it becomes smaller with an increase in temperature due to the increasing number of operative slip systems.[40,41] Sellars et al.[27,28] correlated the combined effect of deformation temperature and strain rate on increase of $\Delta\sigma$ and $\Delta\rho$ in low-carbon steels through Zener–Hollomon parameter (Z) parameter. F_{RXN} values ranging from 1.5 MPa (at 1000 °C, low Z) to 3 MPa (at 850 °C, high Z) were observed depending upon the deformation-processing conditions. The F_{RXN} did not show any dependence on Nb additions at any given deformation temperature for steel B1–B3.

The F_{PIN} was measured using the subgrain boundary model (SBM) of Hansen et al.[1] All input values (r, f_v, l) into the SBM models were experimentally measured in this investigation, with the exception of interfacial energy between the Nb(CN) and austenite. The average mean linear intercept between austenite subgrain boundaries was determined to be 0.50μm from thin-foil TEM studies. An example of a subgrain structure in steel B3, deformed at 950 °C, is shown in Figure 8. The high localized volume fraction of Nb(CN) at austenite

Table II. Quantitative Measurement of Nb(CN) Particle Size and Volume Fraction for Steel B1–B3 as a Function of Deformation Temperature

	Deformation Temperature (°C)	Local Precipitate Distribution Data Experimental Measurement				Precipitate-Pinning Forces (MPa)
		Diam. (nm)	N_S (m^{-2})	N_V (m^{-3})	Local f_v	
Steel B1	850	12.1 ± 2.2	5.3×10^{12}	4.3×10^{20}	4.2×10^{-4}	2.18
	900	16.2 ± 2.3	1.8×10^{12}	1.1×10^{20}	2.5×10^{-4}	0.74
	950	18.6 ± 1.9	6.8×10^{11}	3.7×10^{19}	1.2×10^{-4}	0.27
	1000	16.9 ± 1.9	9.9×10^{10}	5.9×10^{18}	1.5×10^{-5}	0.04
Steel B2	850	17.7 ± 1.9	7.2×10^{12}	4.1×10^{20}	1.2×10^{-3}	2.91
	900	15.7 ± 1.8	5.5×10^{12}	3.5×10^{20}	7.2×10^{-4}	2.24
	950	25.8 ± 2.2	1.6×10^{12}	6.2×10^{19}	5.6×10^{-4}	0.65
	1000	24.0 ± 1.4	4.9×10^{11}	2.1×10^{19}	1.5×10^{-4}	0.20
Steel B3	850	16.2 ± 1.8	1.7×10^{13}	1.1×10^{21}	2.4×10^{-3}	6.97
	900	18.7 ± 2.1	1.1×10^{13}	6.0×10^{20}	2.1×10^{-3}	4.54
	950	26.1 ± 2.1	4.6×10^{12}	1.7×10^{20}	1.6×10^{-3}	1.83
	1000	21.7 ± 1.2	1.9×10^{12}	8.5×10^{19}	4.6×10^{-4}	0.74

All the samples were deformed in a single hit for a true strain, $\varepsilon = 0.40$, isothermally held for 20 secs, and immediately water quenched.
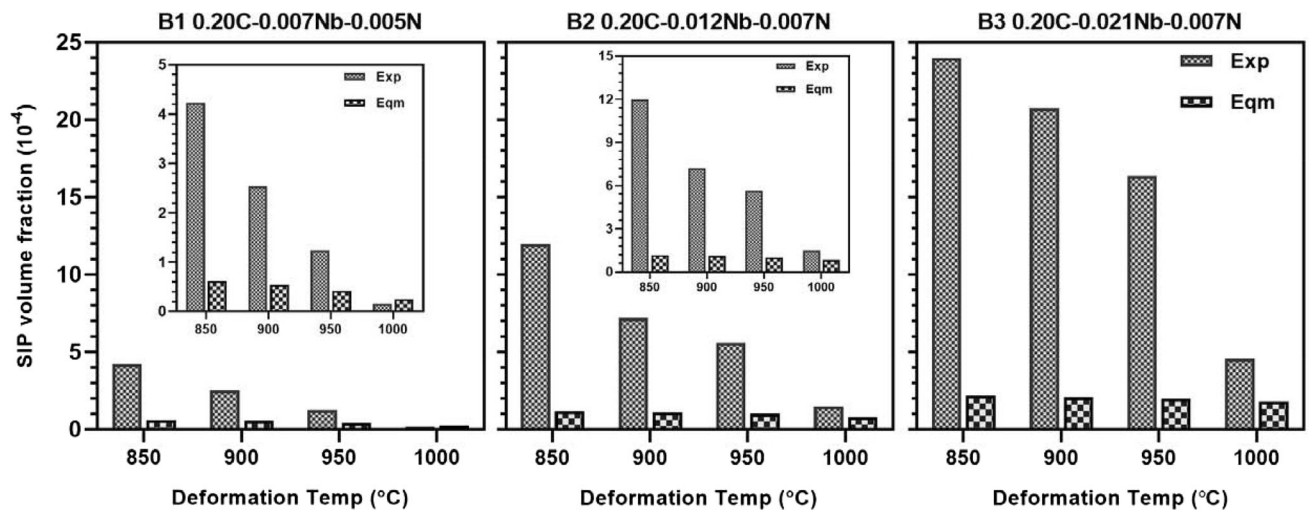

Fig. 10—Volume fraction of Nb(CN) precipitation at different deformation temperatures in steel B1 to B3: Experimental (Exp) measured/$f_{v \, (EXP)}$ versus equilibrium (Eqm)/$f_{v \, (EQM)}$. All the samples were deformed in a single hit for a true strain, $\varepsilon = 0.40$, isothermally held for 20 s, and immediately water quenched.

Table III. Nb Supersaturation (Wt Pct) and Nb Supersaturation Ratio as a Function of Deformation Temperature for Steel B1–B3

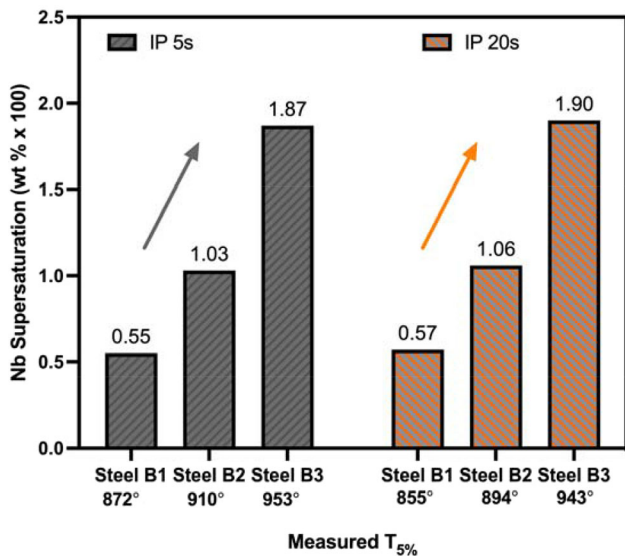| Deformation Temp, °C	Nb Supersaturation (Wt Pct) $[Nb]_{SS} = [Nb]_\gamma - [Nb]_\varepsilon$				Nb Supersaturation Ratio $[Nb]_{SSR} = [Nb]_\gamma / [Nb]_\varepsilon$			
	B0	B1	B2	B3	B0	B1	B2	B3
850	0.0010	0.0058	0.0112	0.0206	2.16	7.93	14.51	25.87
900	0.0003	0.0051	0.0105	0.0199	1.20	4.39	8.03	14.32
950	0.0000	0.0040	0.0094	0.0188	0.70	2.55	4.66	8.31
1000	0.0000	0.0023	0.0078	0.0172	0.42	1.54	2.83	5.04
1050	0.0000	0.0000	0.0053	0.0147	0.27	0.97	1.78	3.17

Fig. 11—Nb supersaturation in austenite at the respective recrystallization-stop temperature ($T_{5\ pct}$) for steel B1–B3 for IP 5 and 20 seconds, respectively. $T_{5\ pct}$ was measured from a fractional softening studies.

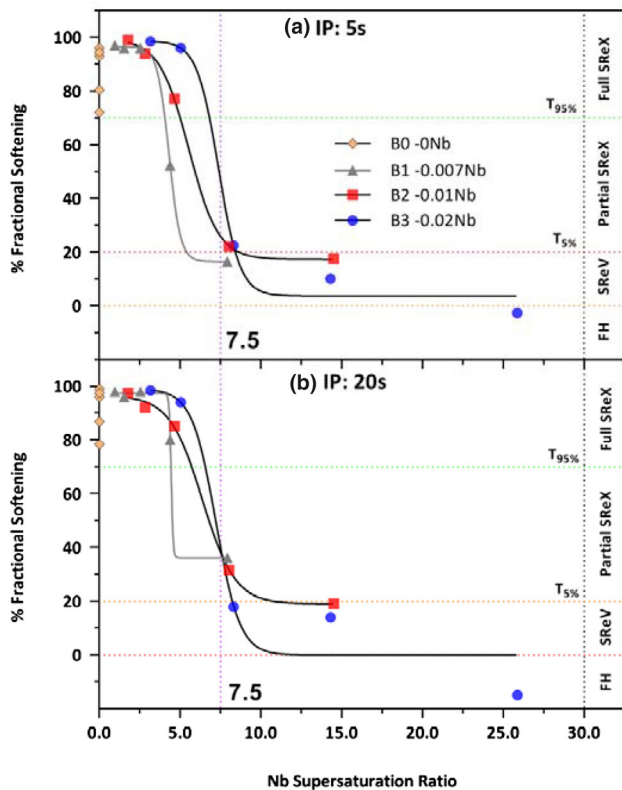Fig. 12—Percent fractional softening for steel B1–B3 as a function of Nb supersaturation Ratio in austenite, $[Nb]_{SSR}$: (a) IP: 5 s and (b) IP: 20 s.

subgrain boundaries is translated into high values of local F_{PIN} for steels B1 to B3.

The F_{PIN} curve in Figure 13 also shows a strong dependence on deformation temperature (*i.e.*, high or low Z condition). This dependence arises because of the

direct influence of the Z parameter on the density of nucleation sites.[28] The measured F_{PIN} also increases with increasing $[Nb]_{SS}$ for steels B1 to B3 at any constant deformation temperature. The high volume fraction of Nb(CN) at prior-austenite grain boundaries is translated into high values of precipitate-pinning force (F_{PIN}). The measured F_{PIN} was significantly higher than those predicted from equilibrium thermodynamics. The F_{PIN} estimation with the SBM model is in agreement with the previous investigation[3,4,27] which validates the acceptance of SBM as the most realistic pinning model.

The interaction between F_{PIN} and F_{RXN} showed good correspondence with fractional softening and quantitative metallography measurements. The recrystallization is retarded only when the precipitate-pinning forces (F_{PIN}) become higher than recrystallization-driving force (F_{RXN}). If the precipitation occurs before the onset of recrystallization, a significant retardation in the recrystallization kinetics is achieved. The accurate estimation of F_{RXN} and F_{PIN} in present work rationalizes the interaction between the recrystallization and precipitation process for investigated steels.

At temperature below the respective $T_{5\ pct}$, the F_{PIN} appears to be of comparable magnitude or higher to the F_{RXN} as illustrated in Figure 13. Static recrystallization was inhibited for steels B1 to B3; whenever, $F_{PIN} \geq F_{RXN}$ corresponded to a critical F_{PIN} of 1.6 MPa. This agreement confirms validity of precipitate pinning in suppressing the static recrystallization of austenite during interpass time by essentially locking the substructure. It also validates that experimentally measured size and volume fraction of localized precipitation were in right range to retard static recrystallization of austenite. For example, steel B2 showed a fully unrecrystallized microstructure at $T_{5\ pct}$ of 900 °C. The pinning force corresponding to an estimated $T_{5\ pct}$ is 1.8 MPa, which exceeded F_{RXN} resulting in a complete retardation of static recrystallization for steel B2. If the $T_{5\ pct}$ is defined as the intersection of F_{PIN} and F_{RXN} curves, then a prediction of $T_{5\ pct}$ = 920 °C is very close to one measured from fraction-softening curves and metallography, $T_{5\ pct}$ = 900 °C.

However, favorable agreement was not obtained in steel B1 as the measured F_{PIN} were lower than F_{RXN} at all deformation temperatures. Steel B1 showed a fully unrecrystallized microstructure at a corresponding $T_{5\ pct}$ of 855 °C. TEM analysis showed the presence of strain-induced precipitation in deformed austenite at 850 °C. However, the measured volume fraction of precipitates was very low which resulted in lower values of local F_{PIN}, equal to 2.18 MP. Also, the local F_{PIN} would have been higher than the current value if the volume fraction of missing fine precipitates (2 nm) was considered.

As mentioned previously, the steels B1 to B3 exhibited a different $[Nb]_{ss}$ at their respective $T_{5\ pct}$. This is summarized in Table IV, along with measured F_{PIN} for steel B1–B3 at respective $T_{5\ pct}$. The table indicates that steel B3 had $[Nb]_{ss}$ of 0.020 at $T_{5\ pct}$ of 943 °C which was 83 pct larger than steel B2. The higher $[Nb]_{ss}$ subsequently resulted in different precipitate volume fraction as shown in Figure 10. Steel B3 exceeded a critical
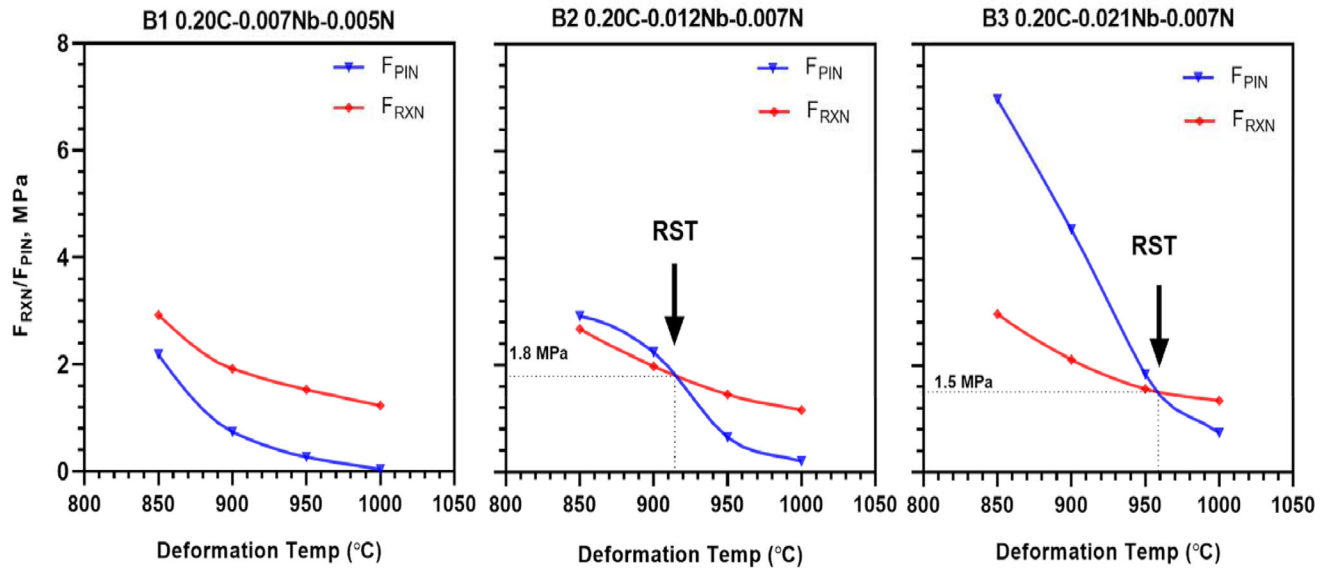
Fig. 13—Interaction between F_{PIN} and F_{RXN} versus deformation temperature for steel B1–B3. Data to the left of the intersection point will result in complete suppression of austenite recrystallization. Data to the right of intersection point will result in partially or fully recrystallized austenite microstructure. All the steels were deformed in a single hit for a true strain, $\varepsilon = 0.40$, isothermally held for 20 s, and immediately water quenched.

pinning force of 1.6 MPa at $T_{5\ pct}$ because of this both coupled phenomena. However, at their respective $T_{5\ pct}$, steel B2 and B1 showed a similar value of F_{PIN} in a range of 1.8–2.5 MPa. Additionally, steels B1–B3 exhibited a critical $[Nb]_{SSR} \geq 7.5$ resulted at their corresponding $T_{5\ pct}$ for $\varepsilon = 0.40$.

As a closing remark, we got quantifiable evidence on the interaction between austenite recrystallization and precipitation as a function of chemistry (*i.e.,* Nb level) and processing parameters (temperature, strain, and strain rate) for a given 0.20 pct C base composition. The findings from the present study have significant importance showing the influence of $[Nb]_{ss}$, critical $[Nb]_{SSR}$, and its associated precipitation potential in retarding the static recrystallization for commodity-grade carbon structural steels. Even the lowest addition of 66 ppm Nb (*i.e.*, ultra-low levels) could retard recrystallization and raised $T_{5\ pct}$ temperature over the base steel composition by as much as 40 °C. Consequently, it is possible to develop a viable deformation schedule to

best benefit even lower strength structural steels through the use of ultra-low Nb additions. Better control of austenite microstructure evolution will improve the mechanical properties of existing low-value commodity-grade products through ferrite grain refinement, which in turn can permit a reduction in other substitutional alloying elements such as Manganese as Nb provides a greater level of strengthening effect even at 66 ppmNb.

V. CONCLUSIONS

1. The isothermal PSC testing proved to be an easy and straightforward method for determining recrystallization-stop ($T_{5\ pct}$) and recrystallization-limit ($T_{95\ pct}$) temperatures. The $T_{5\ pct}$ was associated with 20 pct fractional softening of austenite. A

Table IV.   Comparison of Parameters at $T_{5\ pct}$ for steel B1–B3 (As Measured for This Investigation: $\varepsilon = 0.40$ + Hold Time: 20 s + WQ)

	Parameter	B1	B2	B3
Softening Studies	$T_{5\ pct}$, °C	855	894	943
	aspect ratio	14.01	11.30	10.96
Nb Solubility	bulk Nb Concentration, wt pct	0.0066	0.0121	0.0214
	Nb soluble at 1250 °C, wt pct (1)	0.0066	0.0121	0.0214
	Nb soluble at $T_{5\ pct}$, wt pct (2)	0.0009	0.0014	0.0024
	Nb supersaturation at $T_{5\ pct}$, wt pct (1)-(2)	0.0057	0.0106	0.0190
	Nb supersaturation ratio at $T_{5\ pct}$ (1)/(2)	7.46	8.60	8.95
Interaction	F_{RXN} (MPa)	2.95	1.98	1.56
	F_{PIN} (MPa)	2.18	2.24	1.83
	recrystallization suppressed (yes/no)	YES	YES	YES

Irvine *et al.* [17] solubility equation was used to calculate $[Nb]_\gamma$ and $[Nb]_\varepsilon$.

$T_{5 \text{ pct}}$ of 825, 855, 900, and 943 °C was measured for steels B0, B1, B2, and B3, respectively, for a $\varepsilon = 0.40$ plus isothermal hold time of 20 seconds. The measured $T_{5 \text{ pct}}$ for hold time of 5 seconds was marginally higher (5 °C to 10 °C) than 20 second hold time for similar deformation condition.

2. The $T_{5 \text{ pct}}$ increases with increasing Nb supersaturation in austenite for steel B1–B3. In the present investigation, $T_{5 \text{ pct}}$ increases by 40 °C per 0.006 pct increase in Nb supersaturation over base grade. However, the level of Nb supersaturation was not constant at respective $T_{5 \text{ pct}}$ for steels B1 to B3.

3. The high volume fraction of Nb(CN) at prior-austenite grain boundaries translated into high values of precipitate-pinning force (F_{PIN}). At any given temperature and strain, the local F_{PIN} increases with increasing dilute Nb concentration from steel B1 to B3. A F_{RXN} value ranging from 1.5 MPa (at 1000 °C, low Z) to 3 MPa (at 850 °C, high Z) was observed depending upon Z conditions.

4. The interaction between F_{PIN} and F_{RXN} showed good correspondence with fractional softening and quantitative metallography measurements. At corresponding $T_{5 \text{ pct}}$ (RST), static recrystallization of austenite was inhibited when $F_{PIN} \geq F_{RXN}$, corresponding to critical pinning force of 1.6 MPa. This agreement confirms validity of precipitate pinning in suppressing the static recrystallization of austenite during interpass time by essentially locking the substructure.

5. The Nb supersaturation ratio, $[Nb]_{SSR}$, is a critical factor in determining whether an effective recrystallization and precipitation interaction will take place at particular temperature. The static recrystallization was retarded for steel B1 to B3 whenever the $[Nb]_{SSR}$ exceeded a critical value of 7.5 for any given deformation temperature for a true strain of 0.40.

CONFLICT OF INTEREST

The authors Dr. Bhushan Rakshe and Prof. Eric J Palmiere declare that they have no financial interests. Author Dr. Jitendra Patel is a consultant for CBMM Technology Suisse SA, Switzerland. It is a subsidiary of CBMM based in Geneva and coordinates the company's efforts to develop new niobium applications worldwide.

OPEN ACCESS

REFERENCES

1. S. Hansen, J. Sande, and M. Cohen: *Metall. Trans. A*, 1980, vol. 11A, pp. 387–402.
2. J. Speer and S. Hansen: *Metall. Trans. A*, 1989, vol. 20A, pp. 25–38.
3. O. Kwon and A. DeArdo: *Acta Metall. Mater.*, 1991, vol. 39(4), pp. 529–38.
4. E. Palmiere, C. Garcia, and A. DeArdo: *Metall. Mater. Trans. A*, 1996, vol. 27(4), pp. 951–60.
5. A. le Bon, J. Rofes-Vernis, and C. Rossard: *Met. Sci.*, 1975, vol. 9(1), pp. 36–40.
6. H. Zurob, Y. Brechet, and G. Purdy: *Acta Mater.*, 2001, vol. 49(20), pp. 4183–90.
7. J. Takahashi, K. Kawakami, J. Hamada, and K. Kimura: *Acta Mater.*, 2016, vol. 107, pp. 415–22.
8. M. Suehiro: *ISIJ Int.*, 1998, vol. 38(6), pp. 547–52.
9. World Steel Association: Steel Consumption in Buildings and infrastructure <https://www.worldsteel.org/steel-by-topic/steel-markets/buildings-and-infrastructure.html>.
10. Stronger Steels in the Built Environment (STROBE), RFSR CT 2016-743504, Final Report.
11. B. Donnay and H. Grober: In Conf. Proc. Niobium, Science & Technology. Bridgeville, Pa: Niobium 2001 Limited, 2002.
12. S. Jansto, L. Silvestre and H. Wang: In Conf. Proc. HSLA Steels 2015, Microalloying 2015 & Offshore Engineering Steels 2015, pp. 895–901.
13. S. Jansto: *Metall. and Mater. Trans. B.*, 2013, vol. 45(2), pp. 438–44.
14. S. Jansto: In Conf. Proc. Value Added Niobium Microalloyed Construction Steel, 2012.
15. M. Gómez, S. Medina, A. Quispe, and P. Valles: *ISIJ Int.*, 2002, vol. 42(4), pp. 423–31.
16. Z. Cui, J. Patel and E. Palmiere: In Conf. Proc. HSLA Steels 2015, Microalloying 2015 & Offshore Engineering Steels 2015, pp. 281–87.

17. K. Irvine, F. Pickering, and T. Gladman: *Iron Steel Inst J.*, 1967, vol. 205, pp. 161–82.
18. M. Mirza and C. Sellars: *Mater. Sci. Technol.*, 2001, vol. 17(9), pp. 1133–41.
19. B. Rakshe: PhD thesis, University of Sheffield, UK. <uk.bl.ethos.803677>.
20. R. Thackray, E. Palmiere, and O. Khalid: *Materials*, 2020, vol. 13(15), pp. 3296–3305.
21. R. Higginson and C. Sellars: *Worked Examples in Quantitative Metallography*, The Institute of Materials, London, 2003, pp. 80–100.
22. M. Ashby and R. Ebeling: *Trans. Metall. Soc. AIME*, 1966, vol. 236, pp. 1396–1405.
23. M. Loveday, E. Palmiere, C. Sellars, and M. Winden: *Mater. High Temp.*, 2006, vol. 23(2), pp. 85–118.
24. S. Davenport, N. Silk, C. Sparks, and C. Sellars: *Mater. Sci. Technol.*, 2000, vol. 16, pp. 539–46.
25. O. Kwon and A. DeArdo: *Acta Metall. Mater.*, 1990, vol. 38(1), pp. 41–54.
26. R. Petkovic, M. Luton, and J. Jonas: *Can. Metall. Q.*, 1975, vol. 14(2), pp. 137–45.
27. B. Dutta and E. Palmiere: *Metall. Mater. Trans. A.*, 2003, vol. 34A(6), pp. 1237–47.
28. B. Dutta, E. Palmiere, and C. Sellars: *Acta Mater.*, 2001, vol. 49(5), pp. 785–94.
29. A. Davenport, R. Miner and R. Kot: In Conf. Proc. Hot Deformation of Austenite Ed. J.B. Balance. A.I.M.E., Warrendale, 1986, pp.
30. T. Gladman: *The Physical Metallurgy of Microalloyed Steels*, Institute of Materials, London, 1997, pp. 97–99.
31. E. Valdes and C. Sellars: *Mater. Sci. Technol.*, 1991, vol. 7(7), pp. 622–30.
32. L. Cuddy: In Conf. Proc. Recrystallisation and Grain Growth of Multiphase and Particles Containing Materials. 1980, pp. 317–30.
33. L. Cuddy: In Conf. Proc. Thermomechanical Processing of Microalloyed Austenite, TMS-AIME, New York, 1982, pp. 289–95.
34. H. Nordberg and B. Aronson: *J. Iron Steel Inst.*, 1968, vol. 206, pp. 1263–66.
35. R. Cahn: In Conf. Proc. Recrystallisation, Grain Growth and Textures (ed. H. Margulin), ASM Publication, 1966, pp. 99–127.
36. P. Beck and P. Sperry: *JOM*, 1949, vol. 1(3), pp. 240–41.
37. P. Beck and P. Sperry: *J. Appl. Phys.*, 1950, vol. 21(2), pp. 150–52.
38. J. Bailey and P. Hirsch: In Conf. Proc. Mathematical and Physical Sciences—Series A, Royal Society of London, 1962, 267(1328), pp. 11–30.
39. S. Vervynckt, K. Verbeken, P. Thibaux, and Y. Houbaert: *Mater. Sci. Eng. A*, 2011, vol. 528, pp. 5519–28.
40. A. Kelly, G. Groves, and P. Kidd: *In Crystallography and Crystal Defects*, Wiley, New York, 2000, pp. 198–99.
41. R. Abbaschian, L. Abbaschian, and R. Reed-Hill: *In Physical Metallurgy Principles*, Cengage Learning, USA, 2009, pp. 133–38.